ISSN 0020-1685, Inorganic Materials, 2008, Vol. 44, No. 2, pp. 181–188. © Pleiades Publishing, Inc., 2008.
Original Russian Text © O.Z. Yanchevskii, A.I. Tovstolytkin, O.I. V'yunov, A.G. Belous, 2008, published in Neorganicheskie Materialy, 2008, Vol. 44, No. 2, pp. 226–233.

Structural, Electrical, and Magnetic Properties of $La_{0.7}Ca_{0.3-x}Na_xMnO_{3\pm\gamma}$ Solid Solutions

O. Z. Yanchevskii[a], A. I. Tovstolytkin[b], O. I. V'yunov[a], and A. G. Belous[a]

[a] *Vernadsky Institute of General and Inorganic Chemistry, National Academy of Sciences of Ukraine, pr. Akademika Palladina 32/34, Kiev, 03680 Ukraine*

[b] *Institute of Magnetism, National Academy of Sciences of Ukraine, bul'v. Akademika Vernadskogo 36b, Kiev, 03142 Ukraine*

e-mail: yanchoz@rambler.ru

Received February 26, 2007; in final form, May 25, 2007

Abstract—$La_{0.7}Ca_{0.3-x}Na_xMnO_{3\pm\gamma}$ (LCNM) solid solutions with x = 0, 0.04, 0.06, 0.08, and 0.10 have been synthesized (rhombohedral structure, sp. gr. $R\bar{3}c$). Sodium volatility during sintering is shown to lead to the formation of vacancies on the lanthanum and oxygen sites. $Ca^{2+} \longrightarrow Na^{+}$ substitution does not increase the fraction of Mn^{4+} in LCNM, but the increase in the concentration of lanthanum vacancies with increasing sodium content leads to an increase in ferromagnetic ordering temperature T_C and magnetoresistance, which depend, in addition, on heat-treatment conditions on account of the sodium volatility.

DOI: 10.1134/S0020168508020180

INTRODUCTION

Changes in the charge state of the manganese ions on the B site of ABO_3 perovskite manganites may lead to ferromagnetic ordering and the associated colossal magnetoresistance—a dramatic reduction in resistivity ρ in response to an applied magnetic field [1–3]. The electrical and magnetic properties of the perovskite manganites depend on the formal charge state of the manganese, the average A-cation radius $\bar{R}_A$, the difference in radius between the A cations, and structural details. Ferromagnetic ordering in the manganites is possible at formal charges of Mn from 3.16 to 3.5 [4]. The formal charge state of Mn, in turn, depends on the A-cation charge and oxygen content. In particular, reducing the oxygen content of $LaMnO_{3\pm\gamma}$ and $La_{1-x}Ca_xMnO_{3\pm\gamma}$ suppresses the ferromagnetic behavior of these materials [5, 6]. At the same time, A-site vacancies increase the formal charge of Mn and may substantially raise the ferromagnetic ordering temperature [7, 8]. T_C increases linearly with increasing $\bar{R}_A$, except at high $\bar{R}_A$ values, where nonmonotonic behavior is possible [9, 10]. At a given $\bar{R}_A$ and formal charge on Mn, an increase in the degree of A-site disordering leads to weaker magnetic interaction [11, 12]. A-site disordering can be quantified by $\sigma_A^2 = \sum x_i R_i^2 - \bar{R}_A^2$, where x_i is the fraction of cation i on the A site, and R_i is the ionic radius of cation i [13]. From this viewpoint, it is of interest to study lanthanum calcium sodium manganites, which have small σ_A^2 ($R_{La^{3+}}$ = 1.36 Å, $R_{Ca^{2+}}$ = 1.34 Å, $R_{Na^{+}}$ = 1.39 Å [14]): even low sodium contents must lead to significant changes in the formal charge state of Mn. As shown earlier [15, 16], the high-temperature synthesis of $La_{1-x}Na_xMnO_{3\pm\gamma}$ leads to the formation of sodium vacancies on the A site, which raise T_C. In this paper, we report the synthesis and structural, electrical, and magnetic properties of $La_{0.7}Ca_{0.3-x}Na_xMnO_{3\pm\gamma}$ (LCNM) solid solutions with x = 0, 0.04, 0.06, 0.08, and 0.10.

EXPERIMENTAL

Samples for this investigation were prepared by solid-state reactions, using appropriate mixtures of predried extrapure-grade La_2O_3 and Mn_2O_3 and reagent-grade $CaCO_3$ and Na_2CO_3. The starting mixtures were homogenized by vibration milling with distilled water for 6–8 h using corundum grinding media. Next, the mixtures were dried, screened through a nylon-6 sieve, fired at 1190–1230 K in air for 4 h, and then again homogenized by wet grinding for 4 h. After drying and addition of an aqueous 5% solution of polyvinyl alcohol as a binder, the powder was pressed into disks 10 mm in diameter and 3–4 mm in thickness, which were then sintered at T_{sint} = 1425–1500 K for 1 h in air, without preventing sodium vaporization via packing.

Structural parameters were determined by the Rietveld profile analysis method. X-ray diffraction (XRD) measurements were made on a DRON-4-07

Table 1. Crystal data for $La_{0.7}Ca_{0.3-x}Na_xMnO_{3\pm\gamma}$ ceramic samples sintered at 1475 K

$x_{nominal}$	0	0.04	0.06	0.08	0.10
a, Å	5.474(3)	5.473(2)	5.469(3)	5.471(3)	5.472(1)
c, Å	13.376(7)	13.363(7)	13.366(7)	13.365(5)	13.346(4)
c/a	2.4435	2.4416	2.4439	2.4428	2.4389
V, Å^3	347.1(3)	346.3(3)	346.2(3)	346.3(2)	346.0(2)
O(1): x	0.450(7)	0.431(3)	0.448(7)	0.442(7)	0.445(5)
R_B, %	11.7	11.9	10.5	12.9	10.9
R_f, %	11.2	9.48	8.83	11.3	12.3
Mn–O, Å	1.953(5)	1.955(3)	1.956(6)	1.956(6)	1.955(4)
Mn–O–Mn, deg	163.9(9)	162.2(5)	163.2(9)	162.4(9)	162.3(9)

powder diffractometer (CuK_α radiation). XRD patterns were run in the angular range $2\theta = 10°$–$150°$ in a step-scan mode with a step size $\Delta 2\theta = 0.020°$ and a counting time of 10 s per data point. As external standards, we used SiO_2 (2θ calibration) and Al_2O_3 (NIST SRM 1979 intensity standard). The Mn^{3+} and Mn^{4+} contents of the samples were determined by volumetric analysis [17]; Na was determined by flame spectroscopy using manganite samples dissolved in HCl.

The electrical resistivity ρ of ceramic samples was measured by a four-probe technique at temperatures from 77 to 370 K. The samples were rectangular in shape, $2 \times 3 \times 10$ mm in dimensions. Electrical contacts were made by firing silver paste. Magnetoresistance was determined in applied magnetic fields of up to 1.2 MA/m as

$$\mathrm{MC} = \frac{\rho_0 - \rho_H}{\rho_0} \times 100\%,$$

where ρ_0 is the zero-field resistivity and ρ_H is the resistivity in a magnetic field $H > 0$.

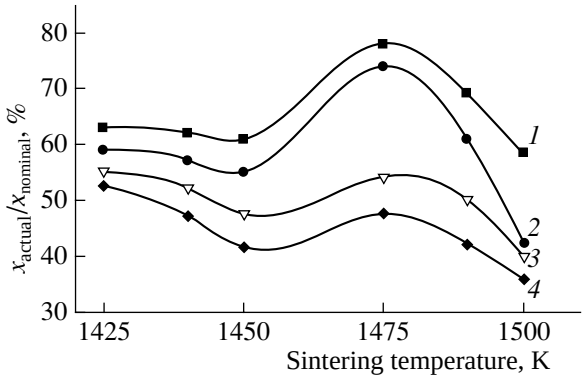

Fig. 1. Effect of sintering temperature on the $x_{actual}/x_{nominal}$ ratio in $La_{0.7}Ca_{0.3-x}Na_xMnO_{3\pm\gamma}$ ceramics: $x_{nominal}$ = (*1*) 0.04, (*2*) 0.06, (*3*) 0.08, (*4*) 0.10.

RESULTS AND DISCUSSION

The XRD data for the LCNM ceramic samples sintered at 1475 K are presented in Table 1. All of the synthesized $La_{0.7}Ca_{0.3-x}Na_xMnO_{3\pm\gamma}$ samples were single-phase and had a rhombohedral structure (sp. gr. $R\bar{3}c$). As seen from Table 1, partial substitution of the larger sized ion Na^+ for calcium produces no systematic changes in unit-cell volume, and the unit cell remains rhombohedral. The present data differ from the results reported by Bhattacharya et al. [18]: in their study, the $x = 0$ sample was orthorhombic (sp. gr. *Pbmn*), and the rhombohedral ($R\bar{3}c$) distortion increased systematically with increasing x. The discrepancy may arise from the difference in synthesis conditions, which are known to influence both the cation and anion nonstoichiometries [7]. The chemical analysis data for sodium in the LCNM samples synthesized at different temperatures are presented in Fig. 1. It can be seen that the relative sodium losses in the ceramics are very large ($0.35 \le x_{actual}/x_{nominal} \le 0.80$) and increase with increasing $x_{nominal}$ (x_{actual} and $x_{nominal}$ are the actual and nominal sodium contents). All of the curves in Fig. 1 have a maximum at a sintering temperature of 1475 K. In an earlier study [16], a small maximum in sodium content was found in the $La_{1-x}Na_xMnO_{3\pm\gamma}$ system at a sintering temperature of 1450 K. Since the vaporization of a volatile component at a given synthesis temperature and duration is limited by the specific surface of the sample, it is reasonable to assume that raising the sintering temperature from 1450 to 1475 K markedly increases the rate of grain growth in the sodium-containing manganites, thereby considerably reducing their specific surface. Further increase in temperature leads to significant sodium losses even in large LCNM grains.

Using chemical analysis for Mn in different oxidation states, we determined the actual compositions of the LCNM samples (Table 2). It follows from the electroneutrality condition for the perovskite (ABO_3) struc-

Table 2. Chemical analysis data and actual compositions of $La_{0.7}Ca_{0.3-x}Na_xMnO_{3\pm\gamma}$ ceramic samples prepared by sintering at 1475 K (η = A-site vacancy)

$x_{nominal}$	$x_{actual}/x_{nominal}$	$\frac{Mn^{4+}}{Mn^{4+}+Mn^{3+}}$	A/B	γ	Actual composition
0		0.363	1	+0.033	$La_{0.7}Ca_{0.3}MnO_{3.033}$
0.04	0.78	0.335	0.9912	–0.007	$La_{0.7}Ca_{0.26}Na_{0.0312}\eta_{0.0088}MnO_{2.993}$
0.06	0.79	0.331	0.9874	–0.0208	$La_{0.7}Ca_{0.24}Na_{0.0474}\eta_{0.0126}MnO_{2.9792}$
0.08	0.54	0.323	0.9632	–0.0469	$La_{0.7}Ca_{0.22}Na_{0.0432}\eta_{0.0368}MnO_{2.9531}$
0.10	0.48	0.315	0.9480	–0.0685	$La_{0.7}Ca_{0.20}Na_{0.0480}\eta_{0.0520}MnO_{2.9315}$

ture that $Ca^{2+} \longrightarrow Na^+$ substitution and, especially, the formation of A-site vacancies as a result of sodium losses must raise the formal charge of Mn. At the same time, the chemical analysis data in Table 2 indicate that the fraction of Mn^{4+} in $La_{0.7}Ca_{0.3-x}Na_xMnO_{3\pm\gamma}$ decreases with increasing $x_{nominal}$. The same is evidenced by the slight increase in Mn–O bond length (Table 1), attesting to a rise in the fraction of Mn^{3+}, which has a larger ionic radius in comparison with Mn^{4+}. As pointed out in earlier studies of $La_{1-x}Na_xMnO_3$ [16] and $La_yA_xMn_wO_3$ solid solutions [19], a reduction in A-cation charge is not always accompanied by an increase in the formal charge of the Mn on the B site. Clearly, the reduction in the formal charge of Mn in LCNM is caused by the increase in the concentration of oxygen vacancies and may also be due to structural requirements. According to Goldschmidt [20], the correspondence of ionic radii with the ideal perovskite (ABO_3) structure can be quantified by the tolerance factor

$$t = \frac{\bar{R}_A + \bar{R}_O}{\sqrt{2}(\bar{R}_B + \bar{R}_O)},$$

where $\bar{R}_A$, $\bar{R}_B$, and $\bar{R}_O$ are the average ionic radii on the A, B, and O sites.

To evaluate the ionic radii in a distorted perovskite structure, we used the formulas derived by Ullmann and Trofimenko [21] and the data in Tables 1 and 2. Calculations were performed for O^{2-} (1.36 Å) in the anion sublattice; La^{3+} (1.36 Å), Ca^{2+} (1.34 Å), and Na^+ (1.39 Å) in the A cation sublattice; and Mn^{3+}_{HS} (0.645 Å), Mn^{3+}_{LS} (0.72 Å), and Mn^{4+}(0.53 Å) in the B cation sublattice [14]. Since Kamata et al. [22] showed that the Mn^{3+} ions in the $La_{0.8}Sr_{0.2}MnO_3$ manganite are present in both high-spin (HS) and low-spin (LS) states, with Mn^{3+}_{HS} : $Mn^{3+}_{LS} \simeq 3:1$, we took $R_{Mn^{3+}} = 0.664$ Å.

At $x = 0$, the structure of $La_{0.7}Ca_{0.3-x}Na_xMnO_{3\pm\gamma}$ is deficient in both A and B cations, and its general formula can be represented as

$$(La_{0.7}Ca_{0.3})_{1-\gamma/3}\square_{La,Ca_{\gamma/3}}(Mn^{3+}_{1-z}Mn^{4+}_z)_{1-\gamma/3}\square_{Mn_{\gamma/3}}O_3,$$

where γ is the oxygen nonstoichiometry coefficient, z is the fraction of Mn^{4+}, and $\square$ stands for a cation vacancy.

The average ionic radii on the A and B sites were evaluated as

$$\bar{R}_A = R_{La_{0.7}Ca_{0.3}}\left[\left(1-\frac{\gamma}{3}\right)+\frac{\gamma}{3}\sqrt[3]{V_f}\right],$$

$$\bar{R}_B = R_{Mn^{3+}_{(1-z)}Mn^{4+}_z}\left[\left(1-\frac{\gamma}{3}\right)+\frac{\gamma}{3}\sqrt[3]{V_f}\right].$$

Here, V_f is the free volume per unit cell, defined by

$$V_f = \frac{V_{meas} - V_{occ}}{V_{meas}},$$

where V_{meas} is the experimentally determined unit-cell volume, and V_{occ} is the occupied volume per unit cell.

For $x > 0$, the structure of $La_{0.7}Ca_{0.3-x}Na_xMnO_{3\pm\gamma}$ is deficient in A cations and oxygen, and its general formula can be represented as

$$(La_{0.7}Ca_{0.3-x}Na_{x-\delta})_{1-\delta}(\square_{La,Ca,Na})_\delta \cdot$$
$$\cdot (Mn^{3+}_{1-z}Mn^{4+}_z)O_{3-\gamma}(\square_O)_\gamma.$$

The average ionic radii on the A and O sites were then evaluated as

$$\bar{R}_A = R_{La_{0.7}Ca_{0.3}Na_{x-\delta}}[(1-\delta)+\delta\sqrt[3]{V_f}],$$

$$\bar{R}_O = R_{O^{2-}}\left[\left(1-\frac{\gamma}{3}\right)+\frac{\gamma}{3}\sqrt[3]{V_f}\right].$$

The average ionic radii on the cation and anion sites, the degree of A-site disordering, free volume per unit cell, actual tolerance factor t_{actual}, and theoretical tolerance factor t_{theor} (without allowance for oxygen vacancies) in the synthesized $La_{0.7}Ca_{0.3-x}Na_xMnO_{3\pm\gamma}$ solid solutions are listed in Table 3. It follows from these data

Table 3. Average ionic radii on the A, B, and O sites, free volume per unit cell, actual and theoretical ($\gamma = 0$) tolerance factors, and degree of A-site disordering in $La_{0.7}Ca_{0.3-x}Na_xMnO_{3\pm\gamma}$ ceramics prepared by sintering at 1475 K

$x_{nominal}$	$\bar{R}_A$, Å	$\bar{R}_B$, Å	$\bar{R}_O$, Å	V_f	t_{actual}	t_{theor}	$\sigma_A^2 \times 10^4$, Å^2
0	1.3486	0.6125	1.360	0.2591	0.9710	0.9710	0.84
0.04	1.3513	0.6190	1.3588	0.2574	0.9689	0.9688	1.24
0.06	1.3504	0.6195	1.3566	0.2603	0.9687	0.9682	1.41
0.08	1.3392	0.6205	1.3525	0.2703	0.9647	0.9637	1.56
0.10	1.3326	0.6216	1.3491	0.2755	0.9622	0.9608	2.09

that the reduction in oxygen site occupancy upon an increase in the concentration of A-site vacancies insures a higher structural stability of LCNM ($t_{actual} > t_{theor}$). This also accounts for the lack of correlation between the charges on the A and B cations in this and earlier studies [7, 16, 19]. It can also be seen from Table 3 that the degree of A-site disordering rises systematically with increasing $x_{nominal}$ (with increasing A-site and oxygen vacancy concentrations). The free volume per unit cell V_f in the LCNM solid solutions has a minimum at $x_{nominal} = 0.04$.

Figure 2 shows the temperature dependences of resistivity for the LCNM ceramics. The characteristic maximum in $\rho(T)$ is associated with the transition from metallic ($d\rho/dT > 0$) to thermally activated ($d\rho/dT < 0$) conduction. The minimum in ρ at $x_{nominal} = 0.04$ can be accounted for by the smallest distortion from cubic symmetry, which favors electronic-band broadening [23]. An increase in $x_{nominal}$ to above 0.4 is accompanied by a jump in resistivity by more than one order of magnitude and a change in the shape of the $\rho(T)$ curves. This points to a transition from one conduction mechanism to another in $La_{0.7}Ca_{0.3-x}Na_xMnO_{3\pm\gamma}$. Partial $Ca^{2+} \longrightarrow Na^+$ substitution shifts the maximum in ρ to higher temperatures and gives rise to another, poorly defined maximum at lower temperatures for $x_{nominal} > 0.6$. The lower temperature maximum in ρ may be interpreted as attesting to an increased role of spin-dependent grain-boundary processes [24] or to a transformation of some of the ferromagnetic conducting phase to a ferromagnetic nonconducting phase.

The temperature dependences of magnetoresistance for LCNM solid solutions synthesized under different conditions are displayed in Fig. 3. These data demonstrate that the height and position of the peak in magnetoresistance depend on sodium content, sintering tem-

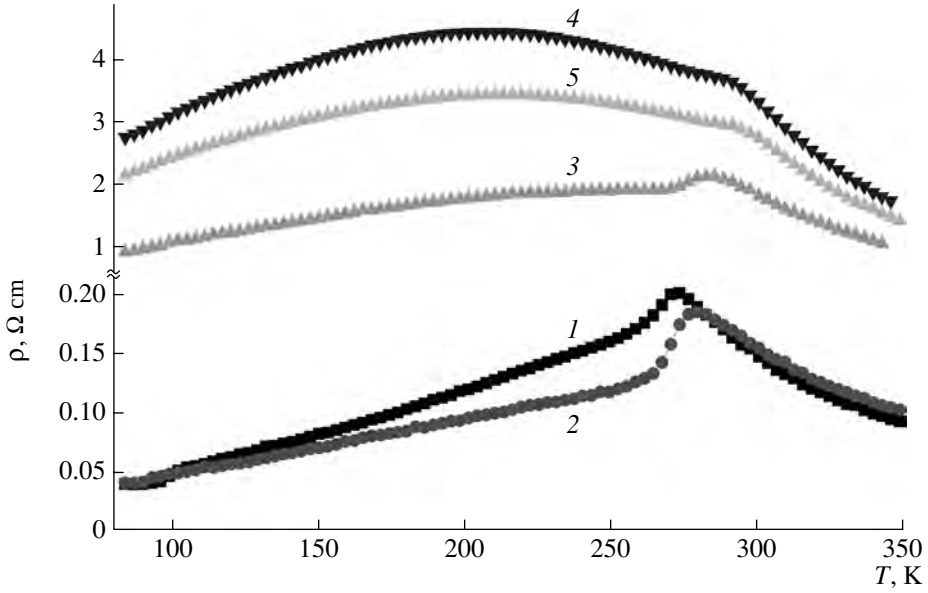

Fig. 2. Temperature dependences of resistivity for $La_{0.7}Ca_{0.3-x}Na_xMnO_{3\pm\gamma}$ ceramics prepared by sintering at 1500 K: $x_{nominal}$ = (*1*) 0, (*2*) 0.04, (*3*) 0.06, (*4*) 0.08, (*5*) 0.10.

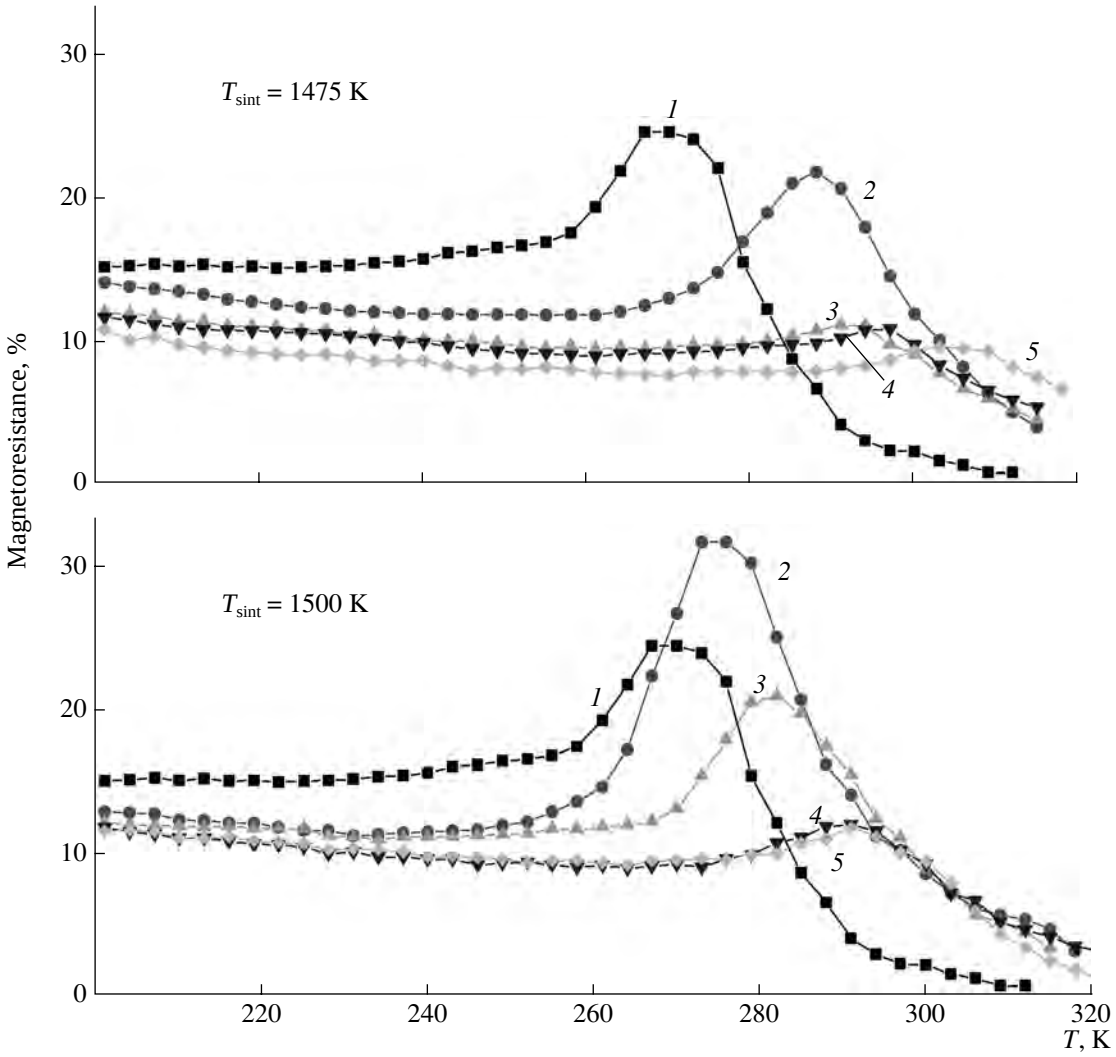

Fig. 3. Temperature dependences of magnetoresistance (H = 1.2 MA/m) for $La_{0.7}Ca_{0.3-x}Na_xMnO_{3\pm\gamma}$ ceramics prepared at different sintering temperatures: $x_{nominal}$ = (*1*) 0, (*2*) 0.04, (*3*) 0.06, (*4*) 0.08, (*5*) 0.10.

perature, and, hence, on the structural perfection of the material. The effect of sintering conditions on the temperature-dependent magnetoresistance of the LCNM ceramics with $x_{nominal}$ = 0.04 and 0.08 is illustrated in Figs. 4 and 5, respectively. Raising the sintering temperature has an advantageous effect on the magnetoresistance of the ceramics at small $x_{nominal}$ and, on the contrary, reduces their magnetoresistive response at large $x_{nominal}$. With increasing $x_{nominal}$, the associated increase in the concentrations of A-site and oxygen vacancies leads not only to a reduction in the magnitude of magnetoresistance but also to growth of the lower temperature maximum.

Since the ferromagnetic ordering temperature of manganites usually coincides with their peak-magnetoresistance temperature [25], we determined T_C as the peak temperature in the magnetoresistance versus T curve. As seen in Fig. 6, the Curie temperature of the LCNM solid solutions depends on both sodium content and synthesis conditions. Partial sodium substitution for calcium in $La_{0.70}Ca_{0.30}MnO_3$ raises T_C in spite of the slight reduction in the formal charge of Mn, which attests to an important role of the structural features of the manganites. At lower concentrations of A-site and oxygen vacancies (T_{sint} = 1475 K), T_C is a stronger function of $x_{nominal}$: $dT_C/x_{nominal}$ is about 3.5 K/mol % Na. On the contrary, increasing the vacancy concentration in LCNM ceramics by raising T_{sint} to 1500 K causes T_C to grow more gradually.

Figure 7 illustrates the effect of sintering temperature on the T_C and maximum magnetoresistance of the $La_{0.7}Ca_{0.3-x}Na_xMnO_{3\pm\gamma}$ ceramics with $x_{nominal}$ = 0.04 and 0.08. It can be seen that the variation of T_C with T_{sint} correlates with that of $x_{actual}/x_{nominal}$ (Fig. 1). Conse-

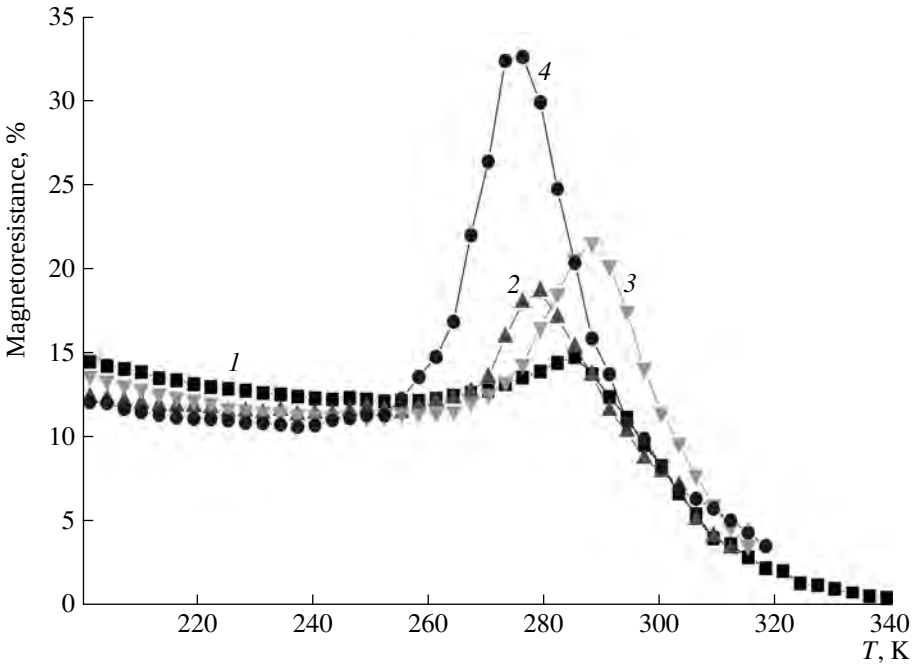

Fig. 4. Temperature dependences of magnetoresistance (H = 1.2 MA/m) for $La_{0.7}Ca_{0.3-x}Na_xMnO_{3\pm\gamma}$ ceramics with $x_{nominal}$ = 0.04 prepared by sintering at (*1*) 1425, (*2*) 1450, (*3*) 1475, and (*4*) 1500 K.

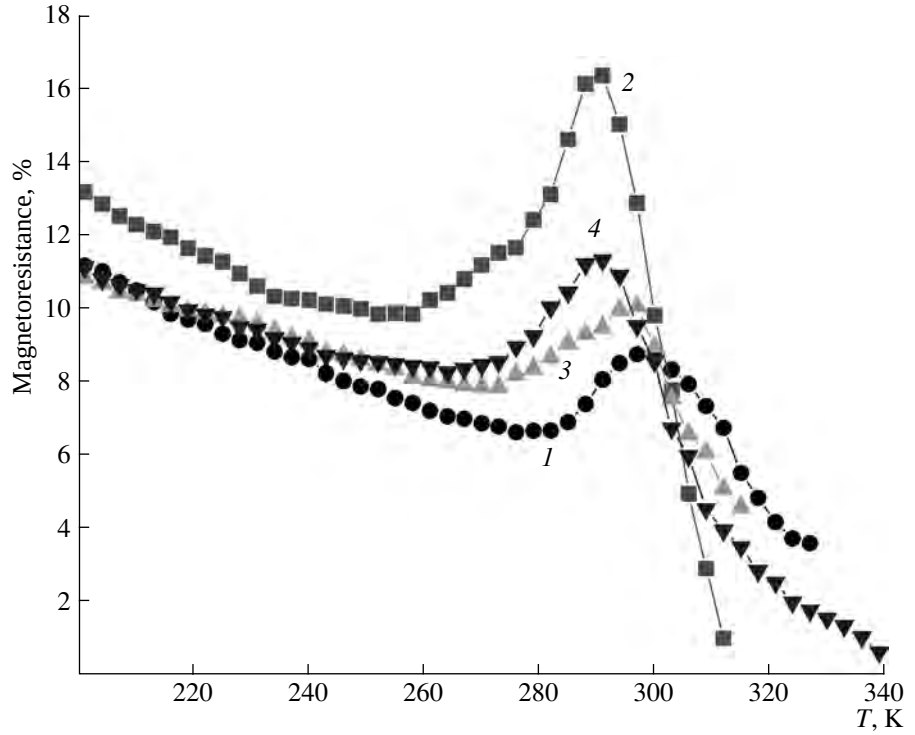

Fig. 5. Temperature dependences of magnetoresistance (H = 1.2 MA/m) for $La_{0.7}Ca_{0.3-x}Na_xMnO_{3\pm\gamma}$ ceramics with $x_{nominal}$ = 0.08 prepared by sintering at (*1*) 1425, (*2*) 1450, (*3*) 1475, and (*4*) 1500 K.

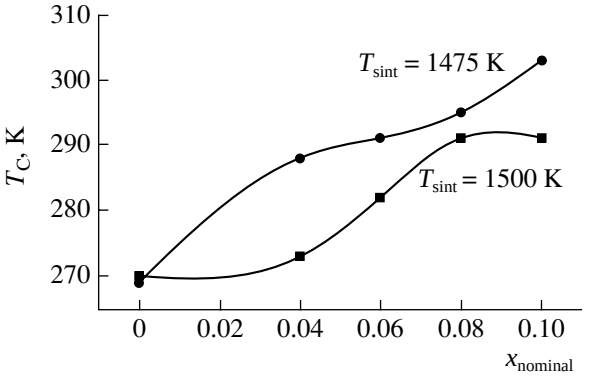

Fig. 6. Effects of nominal sodium content and sintering temperature on the Curie temperature of $La_{0.7}Ca_{0.3-x}Na_xMnO_{3\pm\gamma}$ ceramics.

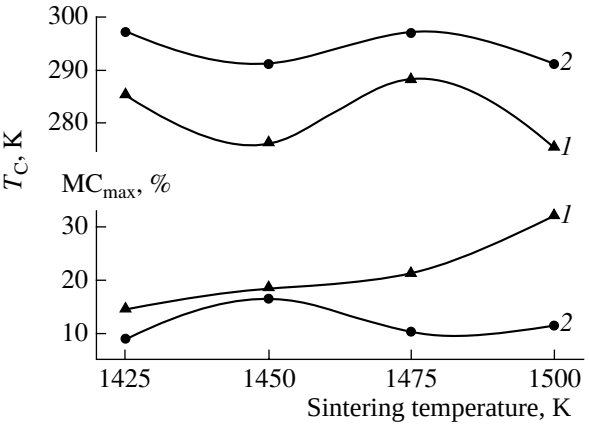

Fig. 7. Effect of sintering temperature on the Curie temperature and maximum magnetoresistance (H = 1.2 MA/m) of $La_{0.7}Ca_{0.3-x}Na_xMnO_{3\pm\gamma}$ ceramics with $x_{nominal}$ = (*1*) 0.04 and (*2*) 0.08.

quently, the ferromagnetic ordering temperature is proportional to the content of sodium, which increases the average ionic radius on the A site, and inversely proportional to the concentration of A-site vacancies. At the same time, the magnetoresistance has a maximum at a certain concentration of A-site vacancies ($0.98 < A/B < 1$), which can be reached by raising the sintering temperature at low sodium contents and by lowering it at high sodium contents. The highest magnetoresistance reached in this study, 32% at $x_{nominal} = 0.04$ and T_{sint} = 1500 K, exceeds that of the parent material $La_{0.7}Ca_{0.3}MnO_{3\pm\gamma}$ by a factor of 1.5 and occurs at a higher temperature. The high magnetoresistance can be understood in terms of the structural features of the manganites: the material with $x_{nominal} = 0.04$ has the minimum free volume per unit cell.

CONCLUSIONS

The $La_{0.7}Ca_{0.3-x}Na_xMnO_{3\pm\gamma}$ solid solutions prepared in this study have a rhombohedral unit cell (sp. gr. $R\bar{3}c$) and contain vacancies on the A and O sites of the perovskite (ABO_3) structure. The concentrations of A-site and oxygen vacancies depend on synthesis conditions. The reduction in the formal charge of Mn with decreasing A-cation charge is associated with the tendency of the perovskite structure to retain its steric stability. The ferromagnetic ordering temperature T_C may increase with decreasing Mn^{4+} content and increasing A-cation disorder. The T_C of LCNM ceramics is proportional to the actual content of sodium, which increases the average ionic radius on the A site, and inversely proportional to the concentration of A-site vacancies, which reduce $\bar{R}_A$. High concentrations of A-site vacancies have an adverse effect on the resistivity and magnetoresistance of LCNM. We found the optimal synthesis temperature and sodium content, which allowed us to notably raise the magnetoresistance of LCNM, from 24 to 32%, and to shift its maximum from 267 K in $La_{0.7}Ca_{0.3}MnO_{3\pm\gamma}$ to 273 K.

REFERENCES

1. Von Helmolt, R., Wecker, J., and Holzapfel, B., et al., Giant Negative Magnetoresistance in PerovskitelikeLa$_{2/3}$Ba$_{1/3}$MnO$_x$ Ferromagnetic Films, *Phys. Rev. Lett.*, 1993, vol. 71, pp. 2331–2333.
2. Tokura, Y., Uruchibara, A., Moritomo, Y., et al., Giant Magnetotransport Phenomena in Filling-Controlled Kondo Lattice SystemLa$_{1-x}$Sr$_x$MnO$_3$, *J. Phys. Soc. Jpn.*, 1994, vol. 63, no. 11, pp. 3931–3935.
3. Ramanathan, M., Tiwary, S.K., Raychaudhuri, A.K., et al., Structure, Electron-Transport Properties, and Giant Magnetoresistance of Hole-Doped $LaMnO_3$ Systems, *Phys. Rev. B: Condens. Matter Mater. Phys.*, 1996, vol. 53, pp. 3348–3358.
4. Schiffer, P., Ramizes, A.P., Bao, W., and Cheong, S.W., Low Temperature Magnetoresistance and the Magnetic Phase Diagram of La$_{1-x}$Ca$_x$MnO$_3$, *Phys. Rev. Lett.*, 1995, pp. 3336–3339.
5. Alonso, J.A., Martinez-Lope, M.J., Casáis, M.T., and Muñoz, A., Magnetic Structures of $LaMnO_{3+\delta}$ Perovskites (δ = 0.11, 0.15, 0.26), *Solid State Commun.*, 1997, vol. 102, no. 1, pp. 7–12.
6. Malavasi, L., Mozzati, M.C., Azzoni, C.B., et al., Role of Oxygen Content on the Transport and Magnetic Properties of La$_{1-x}$Ca$_x$MnO$_{3+\delta}$ Manganites, *Solid State Commun.*, 2002, vol. 123, pp. 321–326.
7. Singh, R.N., Shivakumara, C., Vasanthacharya, N.Y., et al., Synthesis, Structure, and Properties of Sodium or Potassium Doped Lanthanum Orthomanganites from NaCl or KCl Flux, *J. Solid State Chem.*, 1998, vol. 137, pp. 19–27.
8. Gupta, A., McGuire, T.R., Duncombe, P.R., et al., Growth and Giant Magnetoresistance Properties of La-

DeficientLa$_x$MnO$_{3-\delta}$ ($0.67 \le x \le 1$) Films, *Appl. Phys. Lett.*, 1995, vol. 67, no. 23, pp. 3494–3496.

9. Hwang, H.Y., Cheong, S.W., Radoelli, P.G., et al., Lattice Effects on the Magnetoresistance in Doped $LaMnO_3$, *Phys. Rev. Lett.*, 1995, vol. 75, pp. 914–917.
10. Van Roosmalen, J.A.M., Cordfuike, E.H.P., Helmholdt, R.B., and Zandbwergen, H.W., The Defect Chemistry of $LaMnO_{3\pm\delta}$: 2. Structural Aspects of $LaMnO_{3+\delta}$, *J. Solid State Chem.*, 1994, vol. 110, pp. 100–105.
11. Malavasi, L., Mozzati, M.C., Azzoni, C.B., et al., Role of Oxygen Content on the Transport and Magnetic Properties of $La_{1-x}Ca_xMnO_{3+\delta}$ Manganites, *Solid State Commun.*, 2002, vol. 123, pp. 321–326.
12. Nikulin, E.I., Egorov, V.M., Baikov, Yu.M., et al., Electrical Conductivity, Magnetoresistance, and Heat Capacity of Oxygen-Deficient $La_{0.67}Ca_{0.33}MnO_{3-\alpha}$ ($0 \le \alpha \le 0.4$), *Fiz. Tverd. Tela* (S.-Peterburg), 2002, vol. 44, no. 5, pp. 881–887.
13. Rodriguez-Martinez, L.M. and Attfield, J.P., Cation Disorder and Size Effects in Magnetoresistive Manganese Oxide Perovskites, *Phys. Rev. B: Condens. Matter Mater. Phys.*, 1996, vol. 54, pp. R15 622–R15 625.
14. Shannon, R.D., Revised Effective Ionic Radii and Systematic Studies of Interatomic Distances in Halides and Chalcogenides, *Acta Crystallogr., Sect. A: Cryst. Phys., Diffr., Theor. Gen. Crystallogr.*, 1976, vol. 32, no. 5, pp. 751–767.
15. Ye, S.L., Song, W.H., Dai, J.M., et al., Large Room-Temperature Magnetoresistance and Phase Separation in $La_{1-x}Na_xMnO_3$ with $0.1 \le x \le 0.3$, *J. Appl. Phys.*, 2001, vol. 90, no. 6, pp. 2943–2948.
16. Yanchevskii, O.Z., Tovstolytkin, A.I., V'yunov, O.I., et al., Structure and Properties of Nonstoichiometric $La_{1-x}Na_xMnO_3$ Solid Solutions, *Neorg. Mater.*, 2004, vol. 40, no. 7, pp. 853–859 [*Inorg. Mater.* (Engl. Transl.), vol. 40, no. 7, pp. 74–750].
17. Borovskikh, L.V., Mazo, G.A., and Ivanov, V.M., Determination of the Average Oxidation State of Manganese in Mixed Manganites, *Vestn. Mosk. Univ., Ser. 2: Khim.*, 1999, vol. 40, no. 6, pp. 373–374.
18. Bhattacharya, S., Banerjee, A., Pal, S., et al., Transport Properties of Na Doped $La_{1-x}Ca_{x-y}Na_yMnO_3$ Measured in a Pulsed Magnetic Field, *J. Phys.: Condens. Matter*, 2002, vol. 14, pp. 10 221–10 235.
19. Shimura, T., Hayashi, T., Inaguma, Y., and Itoh, M., Magnetic and Electrical Properties of$La_yA_xMn_wO_3$ (A = Na, K, Rb, and Sr) with Perovskite-Type Structure, *J. Solid State Chem.*, 1996, vol. 124, no. 2, pp. 250–263.
20. Goldschmidt, V.M., "Mineralchemie" (Mineral Chemistry), *Fortschr. Mineral.*, 1931, vol. 15, pp. 73–146.
21. Ullmann, H. and Trofimenko, N., Estimation of Effective Ionic Radii in Highly Defective Perovskite-Type Oxides from Experimental Data, *J. Alloys Compd.*, 2001, vol. 316, pp. 153–158.
22. Kamata, H., Yonemura, Y., and Mizusaki, Y., High Temperature Electrical Properties of the Perovskite-Type Oxide $La_{1-x}Sr_xMnO_3$, *J. Phys. Chem. Solids*, 1995, vol. 56, no. 7, pp. 943–950.
23. Roy, S., Guo, Y.Q., Venkatesh, S., and Ali, N., Interplay of Structure and Transport Properties of Sodium-Doped Lanthanum Manganite, *J. Phys.: Condens. Matter*, 2001, vol. 13, pp. 9547–9559.
24. Jin, S.S., Tiefel, T.H., McCormack, M., et al., Thousandfold Change in Resistivity in Magnetoresistive La–Ca–Mn–O Films, *Science*, 1994, vol. 264, no. 5157, pp. 413–415.
25. Mahendiran, R., Mahesh, R., Raychaudhuri, A.K., and Rao, C.N.R., Room Temperature Giant Magnetoresistance in $La_{1-x}Pb_xMnO_3$, *J. Phys. D: Appl. Phys.*, 1995, vol. 28, pp. 1743–1745.

SPELL: ok